Influence of a three-dimensional photonic crystal on the plasmonic properties of gold nanorods

Guanhua Lv,[1] Jinxiang Li,[1] Shao-Long Tie,[2] and Sheng Lan[1,*]

[1]*Guangdong Provincial Key Laboratory of Nanophotonic Functional Materials and Devices, School of Information and Optoelectronic Science and Engineering, South China Normal University, Guangzhou, China*
[2]*School of Chemistry and Environment, South China Normal University, Guangzhou, China*
***slan@scnu.edu.cn*

Abstract: The influence of a three-dimensional (3D) photonic crystal (PC) on the plasmonic properties of gold nanorods (GNRs), which are placed on the surface of the PC, was investigated both numerically and experimentally. The 3D PC formed by closely packed polystyrene spheres was fabricated by using a pressure controlled isothermal heating vertical deposition technique. For a GNR whose longitudinal surface plasmon resonance (LSPR) is located at the bandgap edges of the PC, a dramatic narrowing of the absorption spectrum as well as an enhancement in electric field and thus the absorption was observed. It was suggested that the small group velocities at the bandgap edges of the PC are responsible for the slow decay of the plasmonic mode in the GNR. To confirm the enhancement in the absorption of the GNRs induced by the nearby PC, we examined the two-photon-induced luminescence (TPL) of an assembly of GNRs dispersed on the surface of the PC. Under the excitation of femtosecond laser pulses which was resonant with the LSPR of GNRs, it was found that the excitation intensity necessary for melting GNRs placed on the surface of the PC was nearly one order of magnitude smaller than that for GNRs placed on the surface of a glass slide, in good agreement with the results predicted by the numerical simulations. Our findings indicate the possibility of using PCs to modify the plasmonic and optical properties of GNRs which are quite useful for the practical applications of GNRs such as nanoscale sensors and optical data storage.

References and links

1. J. D. Joannopoulos, R. D. Meade, and J. N. Winn, *Photonic Crystals* (Princeton University Press, 1995).
2. E. Yablonovitch, "Inhibited spontaneous emission in solid-state physics and electronics," Phys. Rev. Lett. **58**(20), 2059–2062 (1987).
3. S. John, "Strong localization of photons in certain disordered dielectric superlattices," Phys. Rev. Lett. **58**(23), 2486–2489 (1987).
4. J. M. Gérard, B. Sermage, B. Gayral, B. Legrand, E. Costard, and V. Thierry-Mieg, "Enhanced spontaneous emission by quantum boxes in a monolithic optical microcavity," Phys. Rev. Lett. **81**(5), 1110–1113 (1998).
5. H. Y. Ryu and M. Notomi, "Enhancement of spontaneous emission from the resonant modes of a photonic crystal slab single-defect cavity," Opt. Lett. **28**(23), 2390–2392 (2003).
6. K. Hennessy, C. Reese, A. Badolato, C. F. Wang, A. Imamoglu, P. M. Petroff, E. Hu, G. Jin, S. Shi, and D. W. Prather, "Square-lattice photonic crystal microcavities for coupling to single InAs quantum dots," Appl. Phys. Lett. **83**(18), 3650–3652 (2003).
7. S.-H. Kwon, H.-Y. Ryu, G.-H. Kim, Y.-H. Lee, and S.-B. Kim, "Photonic bandedge lasers in two-dimensional square-lattice photonic crystal slabs," Appl. Phys. Lett. **83**(19), 3870–3872 (2003).
8. S. Hughes, "Enhanced single-photon emission from quantum dots in photonic crystal waveguides and nanocavities," Opt. Lett. **29**(22), 2659–2661 (2004).

9. W.-Y. Chen, W.-H. Chang, H.-S. Chang, T. M. Hsu, C.-C. Lee, C.-C. Chen, P. G. Luan, J.-Y. Chang, T.-P. Hsieh, and J.-I. Chyi, "Enhanced light emission from InAs quantum dots in single-defect photonic crystal microcavities at room temperature," Appl. Phys. Lett. **87**(7), 071111 (2005).
10. A. Kress, F. Hofbauer, N. Reinelt, M. Kaniber, H. J. Krenner, R. Meyer, G. Bohm, and J. J. Finley, "Manipulation of the spontaneous emission dynamics of quantum dots in two-dimensional photonic crystals," Phys. Rev. B **71**(24), 241304 (2005).
11. E. Viasnoff-Schwoob, C. Weisbuch, H. Benisty, S. Olivier, S. Varoutsis, I. Robert-Philip, R. Houdré, and C. J. M. Smith, "Spontaneous emission enhancement of quantum dots in a photonic crystal wire," Phys. Rev. Lett. **95**(18), 183901 (2005).
12. S. Hughes, "Modified spontaneous emission and qubit entanglement from dipole-coupled quantum dots in a photonic crystal nanocavity," Phys. Rev. Lett. **94**(22), 227402 (2005).
13. D. Englund, D. Fattal, E. Waks, G. Solomon, B. Zhang, T. Nakaoka, Y. Arakawa, Y. Yamamoto, and J. Vucković, "Controlling the spontaneous emission rate of single quantum dots in a two-dimensional photonic crystal," Phys. Rev. Lett. **95**(1), 013904 (2005).
14. D. G. Gevaux, A. J. Bennett, R. M. Stevenson, A. J. Shields, P. Atkinson, J. Griffiths, D. Anderson, G. A. C. Jones, and D. A. Ritchie, "Enhancement and suppression of spontaneous emission by temperature tuning InAs quantum dots to photonic crystal cavities," Appl. Phys. Lett. **88**(13), 131101 (2006).
15. W.-H. Chang, W.-Y. Chen, H.-S. Chang, T.-P. Hsieh, J.-I. Chyi, and T.-M. Hsu, "Efficient single-photon sources based on low-density quantum dots in photonic-crystal nanocavities," Phys. Rev. Lett. **96**(11), 117401 (2006).
16. S. Strauf, K. Hennessy, M. T. Rakher, Y.-S. Choi, A. Badolato, L. C. Andreani, E. L. Hu, P. M. Petroff, and D. Bouwmeester, "Self-tuned quantum dot gain in photonic crystal lasers," Phys. Rev. Lett. **96**(12), 127404 (2006).
17. I. Nikolaev, P. Lodahl, A. van Driel, A. Koenderink, and W. Vos, "Strongly nonexponential time-resolved fluorescence of quantum-dot ensembles in three-dimensional photonic crystals," Phys. Rev. B **75**(11), 115302 (2007).
18. S. Noda, M. Fujita, and T. Asano, "Spontaneous-emission control by photonic crystals and nanocavities," Nat. Photonics **1**(8), 449–458 (2007).
19. J. Li, B. Jia, G. Zhou, C. Bullen, J. Serbin, and M. Gu, "Spectral redistribution in spontaneous emission from quantum-dot-infiltrated 3D woodpile photonic crystals for telecommunications," Adv. Mater. **19**(20), 3276–3280 (2007).
20. A. Brzezinski, J.-T. Lee, J. D. Slinker, G. G. Malliaras, P. V. Braun, and P. Wiltzius, "Enhanced emission from fcc fluorescent photonic crystals," Phys. Rev. B **77**(23), 233106 (2008).
21. M. J. Ventura and M. Gu, "Engineering spontaneous emission in a quantum-dot-doped polymer nanocomposite with three-dimensional photonic crystals," Adv. Mater. **20**(7), 1329–1332 (2008).
22. C. Blum, A. P. Mosk, I. S. Nikolaev, V. Subramaniam, and W. L. Vos, "Color control of natural fluorescent proteins by photonic crystals," Small **4**(4), 492–496 (2008).
23. M. B. Mohamed, V. Volkov, S. Link, and M. A. El-Sayed, "The 'lightning' gold nanorods: fluorescence enhancement of over a million compared to the gold metal," Chem. Phys. Lett. **317**(6), 517–523 (2000).
24. R. A. Farrer, F. L. Butterfield, V. W. Chen, and J. T. Fourkas, "Highly efficient multiphoton-absorption-induced luminescence from gold nanoparticles," Nano Lett. **5**(6), 1139–1142 (2005).
25. H. Wang, T. B. Huff, D. A. Zweifel, W. He, P. S. Low, A. Wei, and J.-X. Cheng, "In vitro and in vivo two-photon luminescence imaging of single gold nanorods," Proc. Natl. Acad. Sci. U.S.A. **102**(44), 15752–15756 (2005).
26. X. Qian, X.-H. Peng, D. O. Ansari, Q. Yin-Goen, G. Z. Chen, D. M. Shin, L. Yang, A. N. Young, M. D. Wang, and S. Nie, "In vivo tumor targeting and spectroscopic detection with surface-enhanced Raman nanoparticle tags," Nat. Biotechnol. **26**(1), 83–90 (2007).
27. F. Gu, L. Zhang, X. Yin, and L. Tong, "Polymer Single-nanowire optical sensors," Nano Lett. **8**(9), 2757–2761 (2008).
28. G. Lu, L. Hou, T. Zhang, W. Li, J. Liu, P. Perriat, and Q. Gong, "Anisotropic Plasmonic Sensing of Individual or Coupled Gold Nanorods," J. Phys. Chem. C **115**(46), 22877–22885 (2011).
29. L. Shao, C. Fang, H. Chen, Y. C. Man, J. Wang, and Q. Lin, "Distinct plasmonic manifestation on gold nanorods induced by the spatial perturbation of small gold nanospheres," Nano Lett. **12**(3), 1424–1430 (2012).
30. P. Zijlstra, P. M. R. Paulo, and M. Orrit, "Optical detection of single non-absorbing molecules using the surface plasmon resonance of a gold nanorod," Nat. Nanotechnol. **7**(6), 379–382 (2012).
31. L. Chen, G.-C. Li, G.-Y. Liu, Q.-F. Dai, S. Lan, S.-L. Tie, and H.-D. Deng, "Sensing the moving direction, position, size, and material type of nanoparticles with the two-photon-induced luminescence of a single gold nanorods," J. Phys. Chem. C **117**(39), 20146–20153 (2013).
32. D. K. Yi, J.-H. Lee, J. A. Rogers, and U. Paik, "Two-dimensional nanohybridization of gold nanorods and polystyrene colloids," Appl. Phys. Lett. **94**(8), 084104 (2009).
33. F. Eftekhari, A. Lee, E. Kumacheva, and A. S. Helmy, "Examining metal nanoparticle surface chemistry using hollow-core, photonic-crystal, fiber-assisted SERS," Opt. Lett. **37**(4), 680–682 (2012).
34. D. Tuyen, A. C. Liu, C. C. Huang, P.-C. Tsai, J. H. Lin, C.-W. Wu, L.-K. Chau, T. S. Yang, Q. Minh, H.-C. Kan, and C. C. Hsu, "Doubly resonant surface-enhanced Raman scattering on gold nanorod decorated inverse opal photonic crystals," Opt. Express **20**(28), 29266–29275 (2012).

35. M. Yu. Tsvetkov, B. N. Khlebtsov, V. A. Khanadeev, V. N. Bagratashvili, P. S. Timashev, M. I. Samoylovich, and N. G. Khlebtsov, "SERS substrates formed by gold nanorods deposited on colloidal silica films," Nanoscale Res. Lett. **8**(1), 250 (2013).
36. W.-S. Kuo, C.-H. Lien, K.-C. Cho, C.-Y. Chang, C.-Y. Lin, P. J. Campagnola, and S.-J. Chen, "Three-dimensional polymer microdevices with gold nanorods," Proc. SPIE **7757**, 77753 (2010).
37. M. Barth, S. Schietinger, S. Fischer, J. Becker, N. Nüsse, T. Aichele, B. Löchel, C. Sönnichsen, and O. Benson, "Nanoassembled plasmonic-photonic hybrid cavity for tailored light-matter coupling," Nano Lett. **10**(3), 891–895 (2010).
38. I. S. Maksymov, "Optical switching and logic gates with hybrid plasmonic–photonic crystal nanobeam cavities," Phys. Lett. A **375**(5), 918–921 (2011).
39. A. Jiménez-Solano, C. López-López, O. Sánchez-Sobrado, J. M. Luque, M. E. Calvo, C. Fernández-López, A. Sánchez-Iglesias, L. M. Liz-Marzán, and H. Míguez, "Integration of gold nanoparticles in optical resonators," Langmuir **28**(24), 9161–9167 (2012).
40. D. Ganta, E. B. Dale, and A. T. Rosenberger, "Maintaining high-Q in an optical microresonator coated with high-aspect-ratio gold nanorods," J. Opt. **15**(10), 105004 (2013).
41. P. Wang, Y. Wang, Z. Yang, X. Guo, X. Lin, X. C. Yu, Y. F. Xiao, W. Fang, L. Zhang, G. Lu, Q. Gong, and L. Tong, "Single-band 2-nm-line-width plasmon resonance in a strongly coupled Au nanorod," Nano Lett. **15**(11), 7581–7586 (2015).
42. C. Sönnichsen, T. Franzl, T. Wilk, G. von Plessen, J. Feldmann, O. Wilson, and P. Mulvaney, "Drastic reduction of plasmon damping in gold nanorods," Phys. Rev. Lett. **88**(7), 077402 (2002).
43. M. R. K. Ali, B. Snyder, and M. A. El-Sayed, "Synthesis and optical properties of small Au nanorods using a seedless growth technique," Langmuir **28**(25), 9807–9815 (2012).
44. Z. Y. Zheng, X. Z. Liu, Y. H. Luo, B. Y. Cheng, D. Z. Zhang, Q. B. Meng, and Y. R. Wang, "Pressure controlled self-assembly of high quality three-dimensional colloidal photonic crystals," Appl. Phys. Lett. **90**(5), 051910 (2007).
45. T.-H. Feng, Q.-F. Dai, L.-J. Wu, Q. Guo, W. Hu, and S. Lan, "Fabrication of high-quality colloidal photonic crystals with sharp band edges for ultrafast all-optical switching," Chin. Phys. B **17**(12), 4533–4540 (2008).
46. A commercial software developed by Lumerical Solution, Inc. (*http://www.lumerical.com*) was used for the numerical simulations.
47. P. Ghenuche, S. Cherukulappurath, T. H. Taminiau, N. F. van Hulst, and R. Quidant, "Spectroscopic mode mapping of resonant plasmon nanoantennas," Phys. Rev. Lett. **101**(11), 116805 (2008).
48. S. Viarbitskaya, A. Teulle, R. Marty, J. Sharma, C. Girard, A. Arbouet, and E. Dujardin, "Tailoring and imaging the plasmonic local density of states in crystalline nanoprisms," Nat. Mater. **12**(5), 426–432 (2013).
49. I. S. Maksymov, L. F. Marsal, and J. Pallares, "Modeling of two-photon absorption in nonlinear photonic crystal all optical switch," Opt. Commun. **269**(1), 137–141 (2007).
50. P. Zijlstra, J. W. M. Chon, and M. Gu, "Five-dimensional optical recording mediated by surface plasmons in gold nanorods," Nature **459**(7245), 410–413 (2009).

1. Introduction

A photonic crystal (PC) is a periodic arrangement of scatterers which forms a periodic modulation in dielectric constant or refractive index in space. Photonic bandgaps, in which the propagation of light is prohibited and the spontaneous emission of atoms is suppressed due to the low density of states (DOS), are expected to appear in a PC if the modulation in refractive index is sufficiently large [1]. Therefore, one of the most important properties of PCs is to modify the DOS in both space and frequency domains. As a result, one can expect to achieve the enhancement of spontaneous emission rate at the band edges or the suppression of spontaneous emission rate in the bandgaps of PCs [2,3]. This topic has been studied extensively for nearly thirty years and semiconductor quantum wells, quantum dots and luminescent molecules are generally used for demonstrating spontaneous emission rate enhancement or suppression [4–22]. By comparing the luminescence lifetime of the testing specimens embedded in a PC with that in the absence of the PC, the enhancement or suppression in spontaneous emission rate induced by the PC can be readily clarified.

In recent years, nanoparticles of noble metals have attracted great interest in the research fields of nanophotonics, biophotonics and plasmonics because of their highly efficient luminescence under either single-photon or multiphoton excitation [23–26]. Among them, gold nanorods (GNRs) have become the focus of many studies owing to the existence of longitudinal surface plasmon resonance (LSPR) which significantly enhance the electric field around GNRs [23]. Under the excitation of femtosecond laser light which is resonant with the LSPRs of GNRs, they can emit highly efficient two-photon-induced luminescence (TPL)

which is quite useful in bioimaging [26]. So far, much effort has been devoted to the study of the plasmonic and optical properties of GNRs and to the exploration of their practical applications. In practice, the strongly enhanced electric field near the surface of a GNR has been applied in surface enhanced Raman scattering (SERS) [26]. In addition, the sensitivity of the LSPR of a GNR to the refractive index of the surrounding environment has been exploited to build nanoscale sensors [27–31].

Apart from the independent studies on PCs and GNRs which are mainly utilized to achieve the enhancement of electric field, the combination of them has been employed to realize various functions. In 2009, Yi *et al.* synthesized colloid PCs in which GNRs were incorporated into the gaps between self-assembled polystyrene (PS) spheres and observed a red shift of the bandgap [32]. Several years later, several research groups reported the use of PCs combined with GNRs to achieve SERS. Eftekhari *et al.* demonstrated the efficacy of hollow core photonic crystal fibers as a SERS platform for investigating the ligand exchange process on the surface of gold nanoparticles (GNPs) on which the SERS signal was found to exhibit a tenfold enhancement [33]. Tuyen *et al.* presented a novel SERS substrate composed of a three-dimensional (3D) polymeric inverse opal PC frame with GNRs and gold nanospheres decorating on the top layer [34]. This SERS substrate produced not only strong but also uniform SERS output due to the well control of GNRs distribution by the periodic PC structure. Tsvetkov *et al.* proposed a new approach to the fabrication of SERS substrates by depositing GNRs on an opal-like PC and demonstrated the existence of optimal PC thickness and GNR deposition density for the maximal SERS effect [35]. On the other hand, the effects of GNRs on the quality factors and other properties of PC resonators were also investigated. Kuo *et al.* fabricated a 3D polyacrylamide microstructure containing GNRs by utilizing femtosecond laser-based two-photon polymerization [36]. The doped GNRs with TPL also act as contrast agent for internal diagnosis of 3D polymer microstructures. Barth *et al.* proposed and demonstrated a hybrid cavity system in which metal nanoparticles are evanescently coupled to a dielectric PC cavity by using a nanoassembly method [37]. They showed that the combined effect of plasmonic field enhancement and high quality factor (Q ≈900) opens new routes for the control of light-matter interaction at the nanoscale. Maksymov proposed a hybrid resonance architecture in which a plasmonic element is coupled to a silicon-on-insulator PC nanobeam cavity operating at telecom wavelengths [38]. A strong cavity mode damping by the plasmonic element offers mechanisms of controlling a probe signal propagating in the nanobeam and it makes possible to create optical switching devices and logic gates. Jiménez-Solano *et al.* investigated the optical absorption of one-dimensional PC resonators containing different types of GNPs and observed strong reinforcement and depletion of the absorption at the designed wavelength ranges [39]. Ganta *et al.* described a method to coat fused-silica microresonators with high-aspect-ratio GNRs and observed that the microresonators maintained an optical quality factor greater than 107 after coating [40]. Such microresonators combine the field enhancement of localized surface plasmon resonances with the cavity-enhanced evanescent components of high-Q whispering-gallery modes and they are useful for plasmonic sensing applications. Very recently, Wang *et al.* reported a dramatic reduction in plasmon resonance line width of a single GNR by coupling it to the whispering gallery modes of a silica microfiber [41]. By using a 1.46-μm-diameter microfiber, they obtained a plasmon resonance as narrow as 2 nm at ~655 nm, with a quality factor up to 330 and extinction ratio of 30 dB. Compared to an uncoupled GNR, the GNR strongly coupled with micofiber offers a 30-fold enhancement in the peak intensity of plasmonic resonant scattering.

So far, most studies on the interplay between PCs and GNRs focus on the influence of GNRs on the optical properties of PCs. In Ref. 41, the whispering gallery modes of a silica microfiber were utilized to modify the plasmonic properties of GNRs. In comparison, less attention has been paid to the influence of PCs on the plasmonic and optical properties of GNRs. When the LSPR of a GNR is excited, the plasmonic mode may decay radiatively or

nonradiatively, corresponding to the scattering and linear absorption of the GNR [42]. In the presence of a PC, the DOS of optical modes at the position of the GNR which is embedded in or placed on the PC will be modified, depending on the relative location of the LSPR with respect to the band edges of the PC. The modification of DOS at the location of the GNR will modify the radiative decay rate of the plasmonic mode (i.e., the scattering) which in turn change the nonradiative decay of the plasmonic mode (i.e., the absorption). Therefore, the study of the influence of a PC on the plasmonic properties of a GNR is not only interesting for fundamental research but also useful for practical application.

In this article, we investigated numerically and experimentally the influence of a 3D PC on the plasmonic and optical properties of GNRs placed on the surface of the PC. It was found that the absorption spectrum of a GNR whose LSPR is resonant with the band edges of the PC is dramatically narrowed and its linear and nonlinear absorption is enhanced. In the experiments, we demonstrated that the melting energy for the GNRs placed on the surface of the PC formed by self-assembled PS spheres is reduced by nearly one order of magnitude as compared with that for the GNRs placed on the glass slide, in good agreement with the prediction of the numerical simulations based on the finite difference time domain (FDTD) technique.

2. Sample preparation, experimental setup and numerical method

The GNRs used in our experiments were synthesized by using a modified seedless method [43]. They possessed an averaged diameter of ~8 nm and a length of ~34 nm, giving rise to a LPSR located at ~780 nm in water or polymer. The 3D PCs composed of closely packed PS spheres with a diameter of 360 nm were fabricated by using a pressure controlled isothermal heating vertical deposition technique [44,45]. High-quality 3D PCs can be obtained by optimizing the fabrication conditions such as the concentration of PS spheres and the vapor pressure. The morphology of the fabricated PCs was characterized by using scanning electron microscopy (SEM) and the transmission spectra of the PCs were measured by using an inverted microscope (Observer A1, Zeiss) connected to a spectrometer (SR-500i-B1, Andor). For optical measurements, GNRs were dispersed on the surface of a PC and a glass slide and the femtosecond (fs) laser light delivered by a Ti: sapphire oscillator (Mira 900S, Coherent) with a pulse duration of 130 fs and a repetition rate of 76 MHz was used to excite GNRs, as schematically shown in Fig. 1. The fs laser light was focused on GNRs by using the 60 × objective (NA = 0.85) of the inverted microscope and the generated TPL was collected by using the same objective and directed to the spectrometer for analysis. The diameter of the excitation spot was estimated to be ~2.0 μm. In the experiments, a large number of GNRs instead of a single GNR will be excited by the fs laser light. The angles between the polarization of the laser light and the long axes of GNRs are randomly distributed between 0° and 90°. In addition, the LSPRs of some GNRs may not be resonant with the laser light. Therefore, the enhancement factor observed in the experiments is the value averaged over many GNRs. In the FDTD simulation [46], a plane wave with its polarization parallel to the long axis of the GNR was normally incident on the PC and a perfectly matched layer boundary was employed to absorb the reflected light. Since the size difference between the PC and the GNR is very large, the mesh size for the PC was chosen to be 2 nm while that for the GNR was set to be 0.5 nm. A non-uniform mesh size generated automatically by the software was used in between them. We simulated the electric field distributions at different wavelengths and derived the absorption of the GNR by calculating the integration of the electric field intensity over the volume of the GNR. At each wavelength, a continuous wave instead of a short pulse was used to calculate the electric field distribution.
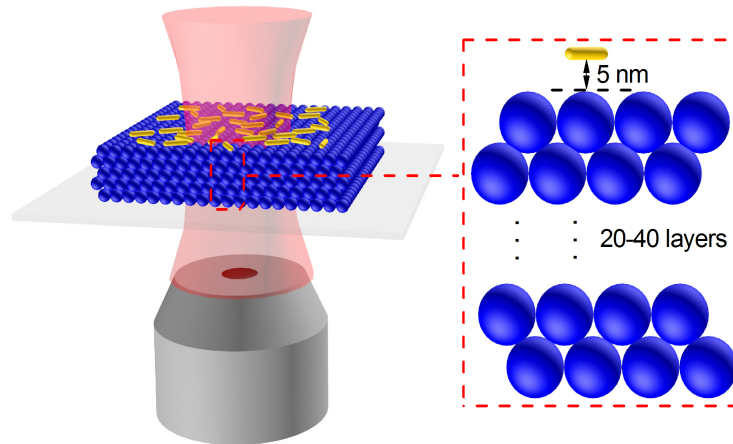
Fig. 1. Schematic showing the excitation of the GNRs dispersed on the surface of a 3D PC formed by self-assembled PS spheres by using focused fs laser light. The magnified graph depicts the detailed structure of the 3D PC and the location of the GNR used in the numerical simulations.

3. Results and discussion

3.1 Effects of a 3D PC on the absorption spectrum of a GNR placed on the surface of the PC

In the numerical simulations, we studied the effects of a 3D PC formed by closely packed PS spheres with a diameter of $d = 360$ nm on the plasmonic properties of a GNR placed on the surface of the PC, as schematically shown in Fig. 1. In the presence of the PC, the calculation of the scattering and extinction of the GNR becomes complicated. Fortunately, one can still derive the absorption of the GNR based on the calculation of the electric field distribution in the GNR in the presence of the PC. Basically, the single-photon absorption of a GNR at a certain wavelength is proportional to the integration of the electric field intensity ($|E|^2$) over the volume of the GNR and the imaginary part of the complex refractive index of gold at this wavelength. In addition, the two-photon-induced absorption (TPA) of the GNR is thought to be proportional to the integration of $|E|^4$ over the volume of the GNR [31,47,48]. Previously, the TPA in a nonlinear PC has been numerically modeled for all-optical switch [49]. In the numerical simulations, we have confirmed that the absorption of a GNR in the absence of the PC can be derived by calculating the electric field distribution inside the GNR. Once the electric field distribution inside the GNR is obtained, one can calculate the integration of $|E|^2$ (or $|E|^4$) over the volume of the GNR and derive the absorption spectrum of the GNR. This method has been previously employed to evaluate the linear and nonlinear absorption spectra of GNRs. In this work, we will focus only on the modification in the absorption spectrum of the GNRs dispersed on the surface of the PC in order to make an easy comparison between the simulation results and the experimental observations.

It has been known that an enhancement of DOS appears at the band edges of a PC in the frequency domain. Accordingly, an enhancement in electromagnetic field appears in the space domain when the wavelength of the incident light is set at the band edges of the PC. In addition, there exist surface states in which the electromagnetic field is localized on the surface of the PC owing to the break of the periodicity [1]. All these features indicate that an enhancement in the electric field is expected for the GNR located near the surface of the PC, leading to an enhancement in the absorption of the GNR. Since the LSPR of the GNR possesses a wide linewidth, the absorption spectrum of the GNR will be modified and the modification depends strongly on the location of the LSPR with respect to the band edges of the PC.

As shown in Fig. 1, we consider a GNR which is located 5 nm above the surface of the PC. This separation is considered to be the average distance for the GNRs dispersed on the surface of the PC in the experiments. If the diameter and length of the GNR are chosen to be 12 and 66 nm, then the LSPR of the GNR appears at ~787 nm which coincides with the first peak of the air band of the PC. By increasing the length of the GNR only to 81 nm, one can shift the LSPR of the GNR to ~880 nm which coincides with the first peak of the dielectric band of the PC. It should be emphasized here that we are considering GNRs in air background and their LSPRs appear at shorter wavelengths as compared with those with the same size but dispersed in water or polymer. Here, the size of the GNR used in the numerical simulations is larger than that used in experiments because the simulation of a 3D system composed of a GNR and a PC is a big challenge for computation resource. Since the volume of the GNR is much smaller than that of the PC, the simulation will require large memory and long time if a small mesh size is chosen for the GNR. Fortunately, we consider only the enhancement factor for the absorption instead of the absolute absorption by using the absorption of the GNR in air as reference. The LSPR (or equivalently the aspect ratio) of the GNRs rather than their size will determine the enhancement factor.
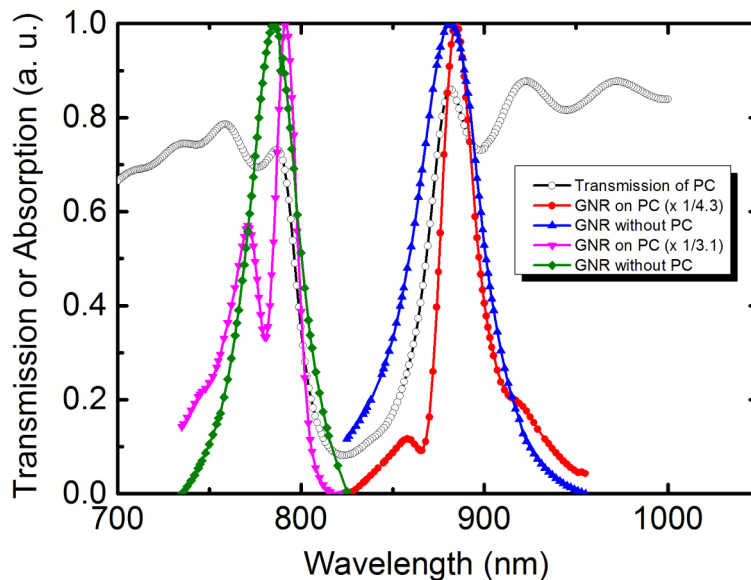

Fig. 2. Absorption spectra calculated for two GNRs placed on the surface of the 3D PC composed of 20 layers of PS spheres. The LSPRs of the GNRs were chosen at the edges of the air band (~787 nm) and dielectric band (~880 nm) of the PC, respectively. The absorption spectra of the same GNRs in air background are also provided for comparison.

In Fig. 2, we present the calculated absorption spectra for two GNRs whose LSPRs are located at the band edges of the air band (~787 nm) and dielectric band (~880 nm) of a 3D PC composed of 20 layers of PS spheres, respectively. The absorption spectra of the same GNRs dispersed in air background are also provided for comparison. A common feature observed in the absorption spectra for the two GNRs is the pronounced narrowing of the linewidth. For the GNR located at ~787 nm, the linewidth of the absorption is reduced from 32 to 14 nm. Similarly, a reduction of linewidth from 42 to 22 nm is also observed for the GNR with LSPR located at 880 nm. In addition, it is remarkable that the peak absorption has been enhanced by 3.1 and 4.3 times at the edges of the air and dielectric band, respectively. A close inspection of the absorption spectra reveals that a slight redshift of the absorption peak appears in the two cases. It means that the absorption peaks of the GNRs do not appear at the first peak of the air or dielectric band. It is also noticed that the original Lorentz line shapes of the

absorption spectra for the GNRs in air are also modified in the presence of the PC. As a result, one can observe small peaks in the absorption spectra of the GNRs on the PC. The physical origins responsible for the redshift of the absorption peak and the small peaks will be discussed later. As mentioned above, the simulation of the system composed of a GNR and a PC is quite time consuming. In Fig. 2, we show the modified absorption spectra calculated for the GNRs placed on the surface of a PC composed of 20 layers of PS spheres. In the numerical simulations, it was found that the enhancement factor at the absorption peak can be increased to ~8.1 by increasing the stacking number of PS spheres in the PC to 40. This value will verified by the experimental observations described later.

3.2 Enhancement in electric field observed for the GNRs placed on the PC

Basically, the enhancement in the absorption observed for the GNRs placed on the surface of the PC originates from the enhancement of the electric field in the GNRs. In Figs. 3(a) and 3(c), we show the electric field intensity ($|E/E_0|^2$) distributions calculated for two GNRs with different aspect ratios in air background. The diameter of the GNRs was fixed at 12 nm while their lengths were chosen to be 66 and 81 nm, respectively. The LSPR of the short GNR appears at ~787 nm which coincides with the first peak of the air band. The LSPR of the long GNR appears at ~880 nm where the first peak of the dielectric band appears. In the presence of the 3D PC composed of 20 layers of PS spheres, the absorption peaks of the two GNRs are red shifted to ~791 and ~882 nm, respectively. We also calculated the electric field intensity distributions at their absorption peaks for the two GNRs in the presence of the PC, as shown in Figs. 3(b) and 3(d). It is apparent that an enhancement in the electric field intensity is observed for the two GNRs when they are placed on the surface of the PC. It is the enhancement in the electric field intensity that leads to the enhancement in the absorption of the GNRs.
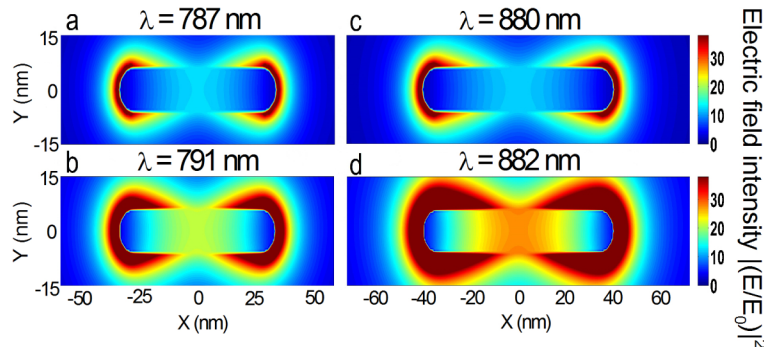

Fig. 3. Electric field intensity ($|E/E_0|^2$) distributions calculated for two GNRs with LSPRs located at 787 nm (a) and 880 nm (c) in the absence of the PC. (b) and (d) show the electric field intensity distributions calculated for the two GNRs placed on the surface of the PC at their absorption peaks appearing at 791 nm and 882 nm, respectively. In all cases, the polarization of the laser light was parallel to the long axis of the GNR.

3.3 Characterization of the 3D PC used in the experiments

As mentioned above, the 3D PC used in our experiments was fabricated by using a pressure controlled isothermal heating vertical deposition technique [44,45]. The concentration of the PS spheres in the aqueous solution was chosen to be 1.0 wt.% while the pressure used in the synthesis of the PC was set to be 45 mmHg. The morphology of the fabricated PC was examined by SEM observation and the top view and cross section of the PC are shown in Figs. 4(a) and 4(b), respectively. It can be seen that PS spheres are closely packed in the PC with more than 40 layers. Although some defects and dislocations are observed in the SEM

images of the PC, we can easily find sufficiently large areas with very good quality on the surface of the PC to carry out the experiments. In Fig. 5, we present the transmission spectra of the PC measured at different locations. A photonic band gap with transmissivity as low as 0.3 is observed in the wavelength region of 780−840 nm. The edge of the air band appears sharper than that of the dielectric band. The transmissivities of both the air and dielectric bands are larger than 0.8, indicating the high quality of the PC. In addition, the three transmission spectra measured at different locations almost coincide, implying the uniformity of the PC. The high quality of the fabricated PC ensures that the influence of the PC on the absorption of the GNRs can be easily observed in the experiments.
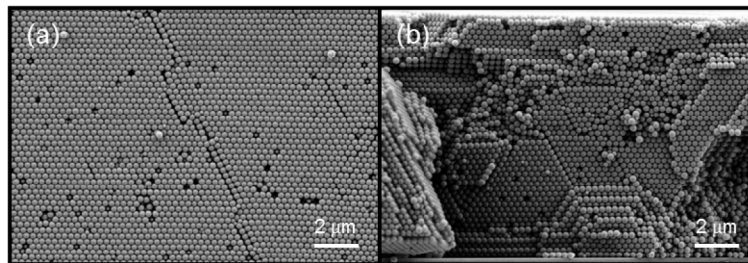

Fig. 4. SEM images of the 3D PC fabricated by using the pressure controlled isothermal vertical deposition technique. (a) Top view. (b) Cross section.
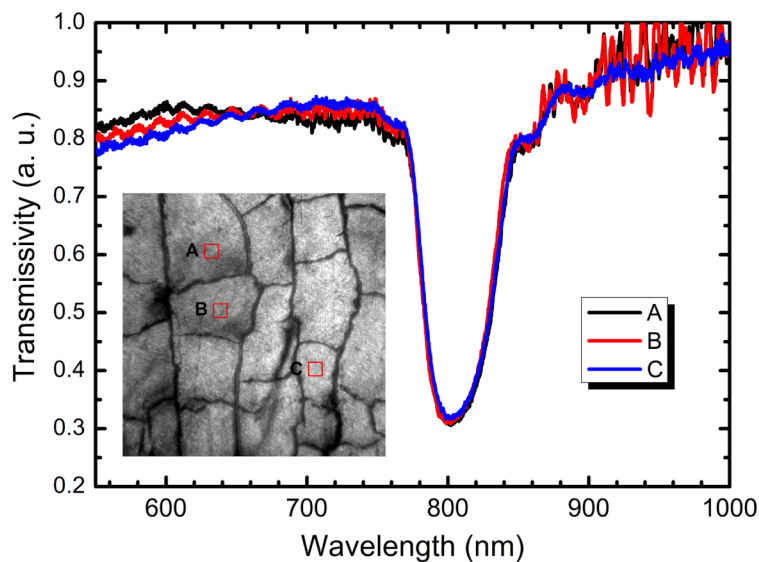

Fig. 5. Transmission spectra of the 3D PC measured at different locations. The CCD image showing the morphology of the PC on which the transmission spectra were obtained.

3.4 Linear and nonlinear absorption of the GNRs under fs laser excitation

When a GNR is excited by a continuous wave (CW) laser at the LSPR peak, the absorption of the GNR is caused mainly by the collision of oscillating electrons with photons, leading to the temperature rise of the GNR. In this case, no transition of electrons between different energy levels is involved [42]. In addition, the intraband absorption in the *sp* conduction band may also contribute to the temperature rise. The absorption induced by these mechanisms is generally referred to as linear absorption because it is proportional to the excitation intensity of the CW laser. However, the situation is different when the GNR is irradiated by a fs laser.

The high peak power of the fs laser pulses may induce a transition of electrons from the *d* band to the *sp* conduction band of gold by simultaneously absorbing two photons (i.e., TPA) if the excitation intensity is large enough [47,48]. After that, the generated electrons will relax to the energy levels just above the Fermi level and recombine with the holes in the *d* band, giving rise to photons which is called TPL. Phonons are emitted during the relaxation of electrons, leading to the temperature rise of the GNR. Apparently, the mechanisms for heat generation are completely different in the linear and nonlinear absorption processes. Basically, the linear absorption is linearly proportional to the excitation intensity while the nonlinear absorption (or TPA) exhibits a quadratic dependence on the excitation intensity. Therefore, the total absorption is dominated by the linear absorption at low excitation intensities and it will be governed by the TPA at high excitation intensities. Basically, one can roughly estimate the excitation intensity at which the TPA becomes equal to the linear absorption based on the cross sections reported previously for the linear and TPA processes [50]. It is estimated to be ~35 mJ/cm^2 for GNRs without a PC. In the presence of a PC, however, both the linear and the TPA processes are greatly enhanced and the later one increases in a larger rate because it is determined by $|E|^4$. As a result, the total absorption may become dominated by the TPA process at a much lower excitation density. In this case, a larger reduction in the melting energy of GNRs placed on the PC will be expected.

3.5 Melting of GNRs with and without the PC under fs laser irradiation

As demonstrated in Section 3.1 by numerical simulation, a modification in the absorption spectrum of a GNR with a specific LSPR can be introduced by placing the GNR on a 3D PC which is formed by closely packed PS spheres. The modification of the absorption spectrum of the GNR is mainly reflected in twofold. One is the narrowing of the LSPR linewidth and the other is the enhancement of the absorption at the LSPR peak. Basically, one can obtain the TPA spectrum of a single GNR by detecting the TPL of the GNR under different excitation wavelengths. From the viewpoint of experiment, however, it is a technological challenge to measure the TPA spectrum a single GNR which is placed on the surface of PC because of many reasons. Apart from the weak TPL of the single GNR, it is quite difficult to accurately to locate the GNR by using dark field microscopy. In our case, the measurement of the TPA spectrum over a wide wavelength range is limited by the tunable wavelength range of the fs laser. In this work, we chose to verify the enhancement in the absorption at the LSPR peak predicted by the numerical calculation and it can be done by exciting a large number of GNRs instead of a single GNR. In our case, we chose GNRs with LSPRs peaking at ~780 nm, as shown in Fig. 6. As can be seen in the inset of Fig. 6, they have an average diameter of ~8 nm and an average length of ~34 nm. In the experiments, we took several droplets of the aqueous solution of GNRs and dropped them on the surface of the PC. Then, the PC was baked at ~100°C for 10 mins to evaporate immediately water. Otherwise, the PC would collapse. After that, we examined again the transmission spectrum of the PC at the position where GNRs were distributed. A comparison of the transmission spectrum before and after the distribution of the GNRs is shown in Fig. 6. A slight increase of the transmissivity from ~0.22 to ~0.28 was observed in the band gap of the PC. In addition, the edge of the air band became less shaper. The change in both the transmissivity and the shape of the transmission spectrum was induced mainly by the intersection between PS spheres during the baking process. Fortunately, such changes do not influence too much the group velocities at the band edges and thus the effects of the PC on the absorption of the GNRs.
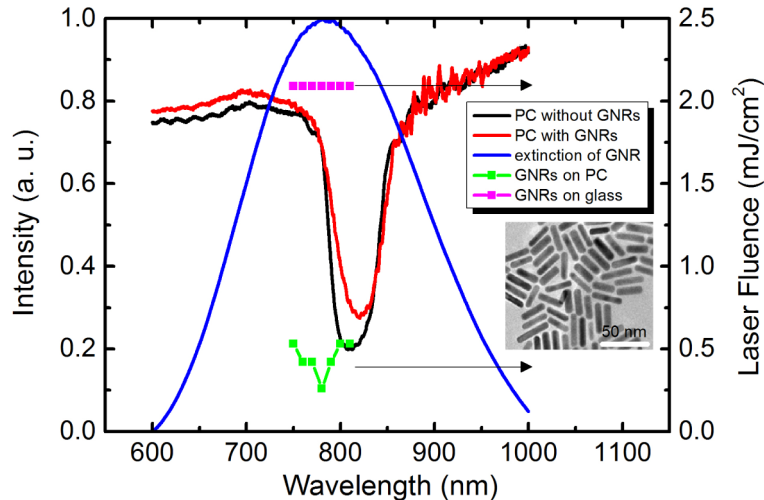
Fig. 6. Transmission spectra of the 3D PC before and after the distribution of the GNRs on the surface. The extinction spectrum of the GNRs is also provided. The laser fluence used to melt the GNRs distributed on the glass slide and those on the PC is compared for different excitation wavelengths. The inset shows the TEM images of the GNRs used in the experiments.

We examined the TPL spectra of the GNRs distributed on the PC at different excitation wavelengths ranging from 750 to 800 nm. This wavelength region covers the edge of the air band which is located at ~780 nm. At each excitation wavelength, we first measured the TPL spectrum of the GNRs at low excitation intensities and recorded the TPL spectrum at a time interval of 2.0 s. In these cases, it was found that the TPL spectrum didn't change with time, implying that no GNRs were melted under these excitation intensities, as shown in Figs. 7(a), 7(c) and 7(e). Then, we increased gradually the excitation intensity and characterized the TPL spectrum of the GNRs with the same procedure. In the experiments, a critical excitation intensity at which a decrease of the TPL intensity with time was observed, as shown in Figs. 7(b), 7(d) and 7(f). It indicates clearly the melting of some GNRs. For excitation intensities larger than the critical value, the reduction in the TPL intensity with increasing time appeared to be more rapidly. It was noticed that the critical excitation intensity exhibited a dependence of the excitation wavelength and the smallest one was achieved at ~780 nm, which coincides with the edge of the air band. For wavelengths shorter or longer than 780 nm, an increase in the critical excitation intensity by a factor of ~2 was observed.

In order to verify the effects of the PC, the same approach was employed to examine the TPL spectra of the GNRs distributed on a glass slide. The measurement results are presented in Fig. 8. It can be seen that the critical excitation intensity at which the TPL intensity decreases with time does not show any dependence on the excitation wavelength. More importantly, it is remarkable that the critical excitation intensity is increased by a factor of ~8 as compared with the minimum excitation intensity observed for the GNRs distributed on the surface of the PC. In principle, the reduction of the critical excitation intensity implies the increase in the absorption of the GNRs. This phenomenon verifies the enhancement in the absorption of the GNRs at their LSPR peaks predicted by the numerical simulations. Since the enhancement factor for a PC composed 40 layers of PS spheres is ~8.1, this result implies that the total absorption of the GNRs is still dominated by linear absorption rather than TPA. For linear absorption, all absorbed energy is converted to heat. However, some absorbed energy is converted to light (i.e., TPL) in TPA. The wavelength-dependent critical excitation intensity, which reflects the wavelength-dependent absorption of the GNRs, is plotted in Fig. 6 for the GNRs distributed on the glass slide and those distributed on the surface of the PC.
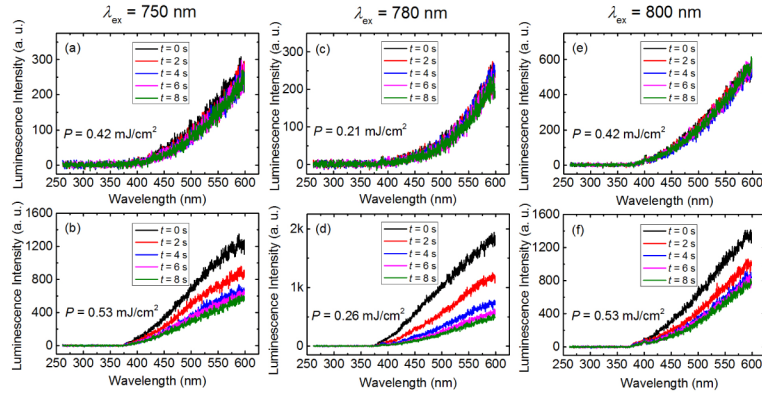
Fig. 7. Evolution of the TPL spectrum of the GNR placed on the surface of the 3D PC with time under the excitation of fs laser light with different excitation wavelengths and intensities. (a) and (b): Evolution of the TPL spectrum measured at 750 nm with excitation densities of 0.42 and 0.53 mJ/cm^2, respectively. (c) and (d): Evolution of the TPL spectrum measured at 780 nm with excitation densities of 0.21 and 0.26 mJ/cm^2, respectively. (e) and (f): Evolution of the TPL spectrum measured at 800 nm with excitation densities of 0.42 and 0.53 mJ/cm^2, respectively.
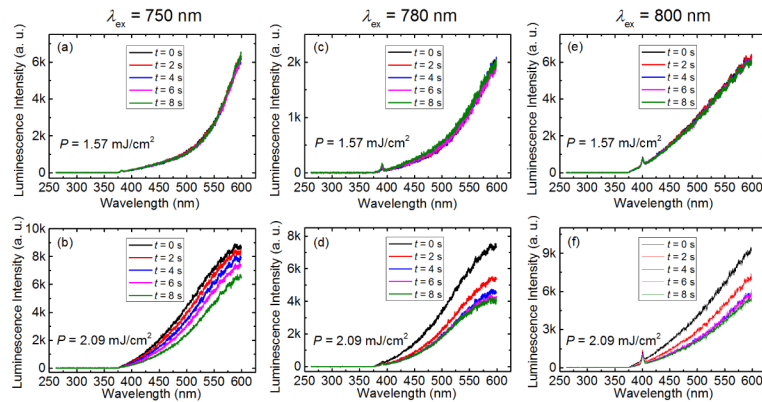

Fig. 8. Evolution of the TPL spectrum of the GNR placed on the surface of the glass slide with time under the excitation of fs laser light with different excitation wavelengths and intensities. (a) and (b): Evolution of the TPL spectrum measured at 750 nm with excitation densities of 1.57 and 2.09 mJ/cm^2, respectively. (c) and (d): Evolution of the TPL spectrum measured at 780 nm with excitation densities of 1.57 and 2.09 mJ/cm^2, respectively. (e) and (f): Evolution of the TPL spectrum measured at 800 nm with excitation densities of 1.57 and 2.09 mJ/cm^2, respectively.

3.6 Influence of the group velocity on the absorption of the GNR placed on the PC

For the GNR placed on the surface of the PC, the electric field intensity inside the GNR will be enhanced due to the existence of the PC. As a result, the absorption of the GNR will be modified. Basically, the LSPR of the GNR may decay in two ways after it has been excited by the incident light. One is scattering and the other is absorption. For a GNR near to a PC, the optical modes coupled to the LSPR of the GNR are modified by the PC. The decay rate of the LSPR into these optical modes will be closely related to the group velocities of these optical modes in the PC. At the edge of the air band, the decay rate of the LSPR into the corresponding optical mode is reduced because of the small group velocity, leading to a longer oscillation of the electrons and an enhancement in the absorption. The longer lifetime of the LSPR is reflected in the narrower linewidth of the LSPR for the GNR placed on the PC.

Basically, the group velocity of a short pulse at a certain wavelength in the PC is reflected in the delay time of the short pulse with respect to the reference pulse propagating in air. The delay times of the short pulses at different wavelengths near the edge of the air band can be determined by the FDTD simulation. In the numerical simulations, the pulse duration was chosen to be 1 ps which corresponds to a linewidth of ~1 nm at 800 nm. In this case, the broadening of the short pulse caused by the dispersion of the PC can be neglected and the delay time of the short pulse can be accurately derived. In Fig. 9(a), we show the relative positions of the short pulses with different wavelengths after transmitting through the PC composed of 20 layers of PS spheres. The position of the reference pulse is also provided. A large delay time of 28.5 fs was observed for the short pulse at 791 nm. In comparison, the delay time for the short pulse at 750 nm was reduced to be 7.2 fs and a superluminal phenomenon was found for the short pulse at 810 nm with a delay time of −14.2 fs.

In Fig. 9(b), we compare the wavelength-dependent delay time calculated for the 1-ps short pulse and the normalized absorption spectrum calculated for the GNR placed on the PC. A qualitative agreement between the two spectra is observed, indicating that the modification in the absorption spectrum of the GNR originating from the modification in the group velocity of the optical modes into which the LSPR of the GNR decays. In other words, the major effect of the PC is to modify the decay rate of the LSPR of the GNR and such a modification leads to the enhancement in the electric field and thus in the absorption of the GNR. In our experiments, we verified the enhancement in the absorption by characterizing the critical excitation intensity for melting the GNR.
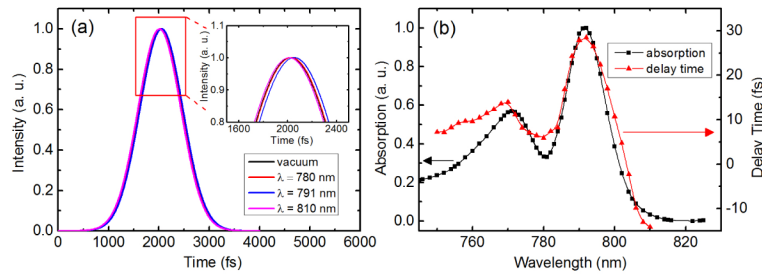

Fig. 9. (a) Pulse shapes detected by a power monitor placed after the PC for three short pulses with different wavelengths in the FDTD simulation. The pulse that transvers the vacuum (i.e., without the PC) is used as reference and its position in time domain is not sensitive to pulse wavelength. The inset shows the magnified pulse peaks which show the advance or delay with respect to the reference pulse. (b) Comparison of the normalized absorption spectrum of the GNR and the spectrum of the time delay induced by the PC.

4. Conclusion

In summary, we have investigated numerically and experimentally the influence of a 3D PC on the plasmonic and optical properties of a GNR placed on the PC. It was found that the absorption spectrum of the GNR whose LSPR is resonant with the band edges of the PC is dramatically narrowed and the linear and nonlinear absorption is enhanced. In the experiments, we demonstrated that the melting energy for the GNRs placed on the surface of the 3D PC formed by self-assembled PS spheres is reduced by a factor of ~8 as compared with that for the GNRs placed on the glass slide, in good agreement with the enhancement in the absorption of the GNRs predicted by the FDTD simulation. Our findings indicate the possibility of using PCs to modify the plasmonic and optical properties of GNRs which are quite useful for the practical applications of GNRs in various fields.

Acknowledgments